arXiv:2112.02895v3 [gr-qc] 29 May 2022

Constraint on parameters of a rotating black hole in Einstein-bumblebee theory by quasi-periodic oscillations

Zejun Wang[1], Songbai Chen[1,2*], Jiliang Jing[1,2 †]
[1] *Department of Physics, Key Laboratory of Low Dimensional Quantum Structures and Quantum Control of Ministry of Education, Synergetic Innovation Center for Quantum Effects and Applications, Hunan Normal University, Changsha, Hunan 410081, People's Republic of China*
[2] *Center for Gravitation and Cosmology, College of Physical Science and Technology, Yangzhou University, Yangzhou 225009, People's Republic of China*

Abstract

We have studied quasi-periodic oscillations frequencies in a rotating black hole with Lorentz symmetry breaking parameter in Einstein-bumblebee gravity by relativistic precession model. We find that in the rotating case with non-zero spin parameter both of the periastron and nodal precession frequencies increase with the Lorentz symmetry breaking parameter, but the azimuthal frequency decreases. In the non-rotating black hole case, the nodal precession frequency disappears for arbitrary Lorentz symmetry breaking parameter. With the observation data of GRO J1655-40, XTE J1550-564, and GRS 1915+105, we find that the constraint on the Lorentz symmetry breaking parameter is more precise with data of GRO J1655-40 in which the best-fit value of the Lorentz symmetry breaking parameter is negative. This could lead to that the rotating black hole in Einstein-bumblebee gravity owns the higher Hawking temperature and the stronger Hawking radiation, but the lower possibility of exacting energy by Penrose process. However, in the range of 1σ, we also find that general relativity remains to be consistent with the observation data of GRO J1655-40, XTE J1550-564 and GRS 1915+105.

PACS numbers: 04.70.Dy, 95.30.Sf, 97.60.Lf

* Corresponding author: csb3752@hunnu.edu.cn
† jljing@hunnu.edu.cn

I. INTRODUCTION

Lorentz invariance has been of great importance in general relativity and the standard model of particle physics. However, according to the development of unified gauge theories and the signals from high energy cosmic rays [1, 2], Lorentz symmetry may spontaneously break in the more fundamental physics at a higher scale of energy. And then studying Lorentz violation is also expected to obtain a deeper understanding of nature. In general, the direct test of Lorentz violation is impossible because their high energy scale is unavailable in the current experimentations. However, recent investigations also show that some signals related to Lorentz violation could emerge at lower energy scales so that their corresponding effects could be observed in experiments [3].

Einstein-bumblebee gravity [4] is a simple effective theory of gravity with Lorentz violation where the spontaneous breaking of Lorentz symmetry is induced by a nonzero vacuum expectation value of bumblebee vector field B_μ with a suitable potential. The black hole solutions in Einstein-bumblebee gravity and the corresponding effects of Lorentz violation have been extensively studied in the past years [5–15]. R. Casana *et al* firstly found an exact solution of a static neutral black hole, and discussed its some classical tests [3]. And then, the gravitational lensing [16], the Hawking radiation [17] and quasinormal modes [18] have been addressed in this black hole spacetime. Moreover, other spherically symmetric black hole solutions, containing global monopole [19], cosmological constant [20], or Einstein-Gauss-Bonnet term [21], and the traversable wormhole solution in the framework of the bumblebee gravity theory [22] have also been found. The cosmological implications of bumblebee gravity model are further investigated in [23] . Furthermore, the rotating black hole solution [24] is also obtained in Einstein bumblebee gravity, and the corresponding shadow [24, 25], accretion disk [26], superradiant instability of black hole [27] and particle's motion [28] around the black hole are studied. A Kerr-Sen-like black hole with a bumblebee field has also been investigated [29]. These investigations are useful for testing Einstein bumblebee theory and detecting the effects caused by the Lorentz symmetry breaking originating from bumblebee vector field.

Quasi-periodic oscillations can be regarded as a promising arena to test the nature of the compact objects, which appear as peaks in the observed X-ray power density spectrum emitted by accreting black hole binary systems [30, 31] and hold important information about gravity in the strong field region. Generally, the frequency range of the quasi-periodic oscillations changes from mHz to hundreds of Hz. There are various theoretical models proposed to account for such peaks in power density spectrum, but the essence of quasi-

periodic oscillations is still unclear at present. The relativistic precession model is a highly regarded model of explaining quasi-periodic oscillations in which the oscillation frequencies are believed to associate with three fundamental frequencies of a test particle around a central object [32–37]. In this model, the azimuthal frequency ν_ϕ and the periastron precession frequency $\nu_{\rm per}$ of the test particle are explained, respectively, as the twin higher frequencies quasi-periodic oscillations. And the nodal precession frequency $\nu_{\rm nod}$ of the particle is identified with the low-frequency quasi-periodic peak in the power density spectrum of low-mass X-ray binaries. Thus, the low-frequency quasi-periodic signal is assumed to be emitted at the same orbit of the test particle where the twin higher frequencies signals are generated. Together with the observation data of GRO J1655-40 [32], the constraint on the black hole parameters in various theories of gravity have been performed by quasi-periodic oscillations within the relativistic precession model [38–51]. The main purpose of this paper is to constrain the Lorentz symmetry breaking parameter for a rotating black hole in Einstein-bumblebee theory of gravity by using of quasi-periodic oscillations with the observation data from GRO J1655-40, XTE J1550-564 and GRS 1915+105 [32, 51–53].

The paper is organized as follows: In Sec.II, we will review briefly the rotating black hole in Einstein-bumblebee theory of gravity [24]. In Sec.III, we study quasi-periodic oscillations in the above black hole spacetime and then make a constraint on the Lorentz symmetry breaking parameter with the observation data of GRO J1655-40, XTE J1550-564 and GRS 1915+105. Finally, we present a summary.

II. A ROTATING BLACK HOLE IN EINSTEIN-BUMBLEBEE THEORY OF GRAVITY

In this section we review briefly a rotating black hole in Einstein-bumblebee theory [24]. In the framework of the bumblebee gravity theory, the spontaneous Lorentz symmetry breaking is induced by a vector B_μ with a non-zero nonzero vacuum expectation value. Through a coupling, the bumblebee vector field B_μ would affect the dynamics of the gravitational field. The action describing such kind of Lorentz symmetry breaking is [3–6]

$$S=\int d^4\sqrt{-g}\Big[\frac{1}{16\pi}(R+\xi B^{\mu\nu}R_{\mu\nu})-\frac{1}{4}B^{\mu\nu}B_{\mu\nu}-V(B_\mu B^\mu\pm b^2)\Big], \tag{1}$$

where ξ is the coupling constant with the dimension M^{-1} and the bumblebee field strength $B_{\mu\nu}=\partial_\mu B_\nu-\partial_\nu B_\mu$. The potential V, inducing Lorentz violation, has a minimum at $B_\mu B^\mu\pm b^2=0$ (where b is a real positive constant), which drives a nonzero vacuum value $\langle B_\mu\rangle=b_\mu$ with $b_\mu b^\mu=\mp b^2$. The signs "$\pm$" in the potential determine whether the field b_μ is timelike or spacelike. Then the nonzero vector background b_μ spontaneously

breaks the Lorentz symmetry [3–6]. The extended vacuum Einstein equations in this model with Lorentz symmetry breaking becomes

$$R_{\mu\nu}-\frac{1}{2}g_{\mu\nu}R=T_{\mu\nu}, \tag{2}$$

with

$$\begin{aligned}T_{\mu\nu} &= B_{\mu\alpha}B^{\alpha}_{\nu}-g_{\mu\nu}\left(\frac{1}{4}B_{\alpha\beta}B^{\alpha\beta}+V\right)-2B_{\mu}B_{\nu}V'+\frac{\xi}{8\pi}\Big[\frac{1}{2}g_{\mu\nu}B_{\alpha}B^{\alpha}-B_{\mu}B^{\alpha}R_{\alpha\nu}-B_{\nu}B^{\alpha}R_{\alpha\mu}\\ &+ \frac{1}{2}\nabla_{\alpha}\nabla_{\mu}(B^{\alpha}B_{\nu})+\frac{1}{2}\nabla_{\alpha}\nabla_{\nu}(B^{\alpha}B_{\mu})-\frac{1}{2}\nabla^{2}(B_{\mu}B_{\nu})-\frac{1}{2}g_{\mu\nu}\nabla_{\alpha}\nabla_{\beta}(B^{\alpha}B_{\beta})\Big].\end{aligned} \tag{3}$$

The Einstein equations (2) admits a rotating black hole solution with a metric [24]

$$\begin{aligned}ds^{2} &= -\left(1-\frac{2Mr}{\rho^{2}}\right)dt^{2}-\frac{4Mar\sqrt{l+1}\sin^{2}\theta}{\rho^{2}}dtd\phi+\frac{\rho^{2}}{\Delta}dr^{2}+\rho^{2}d\theta^{2}\\ &+ \frac{\sin^{2}\theta}{\rho^{2}}\Big[\left(r^{2}+(l+1)a^{2}\right)^{2}-\Delta(l+1)^{2}a^{2}\sin^{2}\theta\Big]d\phi^{2},\end{aligned} \tag{4}$$

where

$$\rho^{2}=r^{2}+(l+1)a^{2}\cos\theta^{2},\qquad \Delta=\frac{r^{2}-2Mr}{l+1}+a^{2}. \tag{5}$$

Here M is the ADM mass and a is the spin parameter of black hole. The form of the bumblebee field is $b_{\mu}=(0,b\rho,0,0)$, and the parameter $l=\xi b^{2}$ depends on the spontaneous Lorentz symmetry breaking of the vacuum of the Einstein-bumblebee vector field. The determinant of the metric (4) is $g=-(l+1)\rho^{4}\sin^{2}\theta$ and then the metric becomes degenerate when $l=-1$. Thus, in order to maintain its Lorentz signature, one must have $l>-1$, which means that the coupling ξ should be restricted to $\xi>-\frac{1}{b^{2}}$. As in the Kerr black hole case, the singularity lies at $\rho^{2}=0$ and the horizon locates at $\Delta=0$. However, the horizon radius becomes

$$r_{\pm}=M\pm\sqrt{M^{2}-(l+1)a^{2}}, \tag{6}$$

which depends on the spontaneous Lorentz symmetry breaking parameter l. With the increase of the absolute value of l, the outer horizon radius decreases for the positive l and increases for the negative one. Thus, comparing with the usual Kerr black hole, the negative l leads to that the rotating black hole (4) owns the higher Hawking temperature and the stronger Hawking radiation [24] . Moreover, for a rotating black hole (4), its mass and spin parameters must satisfy $\frac{|a|}{M}\leq\frac{1}{\sqrt{l+1}}$. The negative l broadens the range of black hole spin parameter so that $|a|>M$, but the positive l shortens the range of a, which differs quite from the Kerr case in general relativity.

III. CONSTRAINT ON PARAMETERS OF A ROTATING BLACK HOLE IN EINSTEIN-BUMBLEBEE THEORY BY QUASI-PERIODIC OSCILLATIONS

In this section, we will apply quasi-periodic oscillations to make a constraint on parameters of a rotating black hole (4) in Einstein-bumblebee theory. For a general stationary and axially symmetric spacetime, the metric of a rotating black hole with bumblebee field (4) can be written as a common form

$$ds^2 = g_{tt}dt^2 + g_{rr}dr^2 + 2g_{t\phi}dtd\phi + g_{\theta\theta}d\theta^2 + g_{\phi\phi}d\phi^2. \tag{7}$$

Obviously, the metric coefficients in Eq. (4) are independent of the coordinates t and ϕ. Thus, the geodesic motion of particle in the black hole spacetime (4) exists two conserved quantities, i.e., the specific energy at infinity E and the conserved z-component of the specific angular momentum at infinity L_z, and the forms of E and L_z can be expressed as

$$E = -p_t = -g_{tt}\dot{t} - g_{t\phi}\dot{\phi}, \qquad L_z = p_\phi = g_{t\phi}\dot{t} + g_{\phi\phi}\dot{\phi}. \tag{8}$$

With above two conserved quantities, the timelike geodesics can be further simplified as

$$\dot{t} = \frac{g_{\phi\phi}E + g_{t\phi}L_z}{g_{t\phi}^2 - g_{tt}g_{\phi\phi}}, \tag{9}$$

$$\dot{\phi} = \frac{g_{t\phi}E + g_{tt}L_z}{g_{tt}g_{\phi\phi} - g_{t\phi}^2}, \tag{10}$$

$$g_{rr}\dot{r}^2 + g_{\theta\theta}\dot{\theta}^2 = V_{eff}(r, \theta; E, L_z), \tag{11}$$

where $V_{eff}(r, \theta; E, L_z)$ is the effective potential with the form

$$V_{eff}(r, \theta; E, L_z) = \frac{E^2 g_{\phi\phi} + 2EL_z g_{t\phi} + L_z^2 g_{tt}}{g_{t\phi}^2 - g_{tt}g_{\phi\phi}} - 1. \tag{12}$$

Here the overhead dot represents a derivative with respect to the affine parameter λ. The effective potential determines the orbit of the particle. The form of potential (12) in the equatorial plane becomes

$$V_{eff}(r, \frac{\pi}{2}; E, L_z) = \frac{[r^3 + (r+2M)(l+1)a^2]E^2 - 4aM\sqrt{l+1}EL_z - (r-2M)L_z^2}{r[r^2 - 2Mr + (l+1)a^2]} - 1. \tag{13}$$

Actually, the radial component of the timelike geodesic equations

$$\frac{d}{d\lambda}(g_{\mu\nu}\dot{x}^\nu) = \frac{1}{2}(\partial_\mu g_{\nu\rho})\dot{x}^\nu\dot{x}^\rho, \tag{14}$$

can be written as [32–35]

$$\frac{d}{d\lambda}(g_{rr}\dot{r}) = \frac{1}{2}\Big[(\partial_r g_{tt})\dot{t}^2 + 2(\partial_r g_{t\phi})\dot{t}\dot{\phi} + (\partial_r g_{\phi\phi})\dot{\phi}^2 + (\partial_r g_{rr})\dot{r}^2 + (\partial_r g_{\theta\theta})\dot{\theta}^2\Big]. \tag{15}$$

We here consider only the case where a particle moving along a circular orbit in the equatorial plane, i.e., $r = r_0$ and $\theta = \pi/2$, which means that $\dot{r} = \dot{\theta} = \ddot{r} = 0$. Thus, for the circular equatorial orbit case, Eq.(15) can be simplified as

$$(\partial_r g_{tt})\dot{t}^2 + 2(\partial_r g_{t\phi})\dot{t}\dot{\phi} + (\partial_r g_{\phi\phi})\dot{\phi}^2 = 0, \tag{16}$$

which gives the orbital angular velocity Ω_ϕ of a particle moving along the circular orbits

$$\Omega_\phi = \frac{d\phi}{dt} = \frac{-g_{t\phi,r} \pm \sqrt{(g_{t\phi,r})^2 + g_{tt,r}g_{\phi\phi,r}}}{g_{\phi\phi,r}} = \pm\frac{g_{tt,r}}{\sqrt{(g_{t\phi,r})^2 + g_{tt,r}g_{\phi\phi,r}} \pm g_{t\phi,r}}, \tag{17}$$

here the sign is $+(-)$ for co-rotating (counter-rotating) orbits. The corresponding azimuthal frequency $\nu_\phi = \Omega_\phi/(2\pi)$. For a timelike particle moving along circular orbits in the equatorial plane, the timelike conditions $g_{\mu\nu}\dot{x}^\mu\dot{x}^\nu = -1$ gives another relationship between $\dot{t}$ and $\dot{\phi}$

$$g_{tt}\dot{t}^2 + 2g_{t\phi}\dot{t}\dot{\phi} + g_{\phi\phi}\dot{\phi}^2 = -1. \tag{18}$$

From two independent equations (16) and (18), one can obtain

$$\dot{t} = \frac{1}{\sqrt{-g_{tt} - 2g_{t\phi}\Omega_\phi - g_{\phi\phi}\Omega_\phi^2}}. \tag{19}$$

Together with Eq.(8), one can find that the specific energy E and the conserved z-component of the specific angular momentum L_z are expressed respectively as [32–35]

$$\begin{aligned} E &= -\frac{g_{tt} + g_{t\phi}\Omega_\phi}{\sqrt{-g_{tt} - 2g_{t\phi}\Omega_\phi - g_{\phi\phi}\Omega_\phi^2}}, \\ L_z &= \frac{g_{t\phi} + g_{\phi\phi}\Omega_\phi}{\sqrt{-g_{tt} - 2g_{t\phi}\Omega_\phi - g_{\phi\phi}\Omega_\phi^2}}. \end{aligned} \tag{20}$$

The radius of circular orbit r_0 in the equatorial plane can be given by the conditions

$$V_{eff}(r_0, \frac{\pi}{2}; E, L_z) = 0, \qquad \left.\frac{dV_{eff}(r, \frac{\pi}{2}; E, L_z)}{dr}\right|_{r=r_0} = 0. \tag{21}$$

Making use of these two conditions, we can obtain the specific angular momentum L_z of a particle moving along the circular orbit r_0 in the equatorial plane

$$L_z = \pm\sqrt{3(E^2-1)[r_0^2 + (l+1)a^2] + 4Mr_0}, \tag{22}$$

and find that the corresponding circular orbit r_0 satisfies

$$(1-E^2)r_0^3 + M(3E^2-4)r_0^2 + 4M^2r_0 + Ma^2(l+1)(2E^2-1) - 2aEM\sqrt{(l+1)W} = 0, \tag{23}$$

with

$$W = 3(E^2-1)r_0^2 + 4Mr_0 + a^2(E^2-1)(l+1). \tag{24}$$

It indicates the radius of circular orbit r_0 is a function of four independent parameters, i.e., M, a, l and the particle's energy E. Thus, the circular orbit with certain fixed radius r_0 could exists for a particle in a rotating black hole spacetime (4) in Einstein-bumblebee theory since there are four adjustable parameters. In Fig. (1), we present the equivalent surface of the circular orbit radius $r_0 = 6.5$ in the parameter space a, l and E (here we set $M = 1$), which shows that it is possible for the existence of circular orbit with $r_0 = 6.5$ for fixed l and a through the choice of a proper parameter E. For the non-rotating black hole (i.e., $a = 0$), we find that

$$r_0 = \frac{[(3E^2-4) \pm E\sqrt{9E^2-8}]M}{2(E^2-1)}, \tag{25}$$

which is independent of the parameter l. This can be explained by a fact that the potential (13) does not depend on l as $a = 0$. The radius r_0 has positive roots as $E \geq \frac{2\sqrt{2}}{3}$ and no any real root as $E < \frac{2\sqrt{2}}{3}$. These positive roots increase with the black hole mass M. With the increase of E, the root with the sign "+" decreases in the allowable range of E, but the root with the sign "−" increases as $\frac{2\sqrt{2}}{3} \leq E < 1$ and it becomes negative as $E > 1$. For the rotating case with $a \neq 0$, we can not obtain the analytical form of r_0. From Eq.(23), we can get the partial derivative of r_0 with respect to M, a, l and E, respectively.

$$\left.\frac{\partial r_0}{\partial M}\right|_{a,l,E} = \frac{[(3E^2-4)r_0^2 + 8Mr_0 + a^2(l+1)(2E^2-1)]\sqrt{W} - 2aE\sqrt{l+1}(2Mr_0+W)}{[3(E^2-1)r_0+2M][(r_0-2M)\sqrt{W}+2aME\sqrt{l+1}]}, \tag{26}$$

$$\left.\frac{\partial r_0}{\partial a}\right|_{M,l,E} = -\frac{2M\sqrt{l+1}[EW-(2E^2-1)a\sqrt{W(l+1)}+a^2E(E^2-1)(l+1)]}{[3(E^2-1)r_0+2M][(r_0-2M)\sqrt{W}+2aME\sqrt{l+1}]}, \tag{27}$$

$$\left.\frac{\partial r_0}{\partial l}\right|_{M,a,E} = -\frac{aM[EW-(2E^2-1)a\sqrt{W(l+1)}+a^2E(E^2-1)(l+1)]}{\sqrt{l+1}[3(E^2-1)r_0+2M][(r_0-2M)\sqrt{W}+2aME\sqrt{l+1}]}, \tag{28}$$

$$\left.\frac{\partial r_0}{\partial E}\right|_{M,a,l} = -\frac{2aM\sqrt{l+1}[3E^2r_0^2+a^2E^2(l+1)+W-2aE\sqrt{W(l+1)}]+2Er_0^2(r_0-3M)\sqrt{W}}{[3(E^2-1)r_0+2M][(r_0-2M)\sqrt{W}+2aME\sqrt{l+1}]}. \tag{29}$$

The above formulas indicate that it is not easy to determine the signs of these partial derivative determine, which means that the change of circular orbital radius r_0 with M, a, l and E becomes very complicated in the rotating black hole case. However, formulas (27) and (28) tell us that the dependent behavior of r_0 on the parameter l is qualitatively similar to that on the spin parameter a. In Fig.(2), we present the change of circular orbital radius r_0 with M, a, l and E for some fixed parameters. For the chosen parameters, as the particle's energy $E < 1$, there exist four circular orbits: a stable co-rotating orbit, a stable counter-rotating orbit, an unstable counter-rotating orbit and an unstable co-rotating orbit, which are marked in the brown, blue, black and red lines, respectively. While as $E \geq 1$, there are two circular orbits, which correspond to the

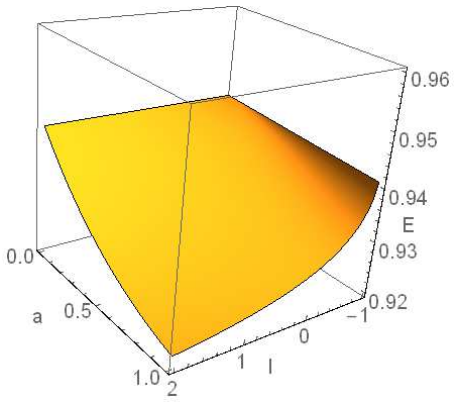


FIG. 1: The equivalent surface of the circular orbit radius $r_0 = 6.5$ in the parameter space (a, l, E) in the rotating black hole spacetime (4) in Einstein-bumblebee theory. Here we set $M = 1$.

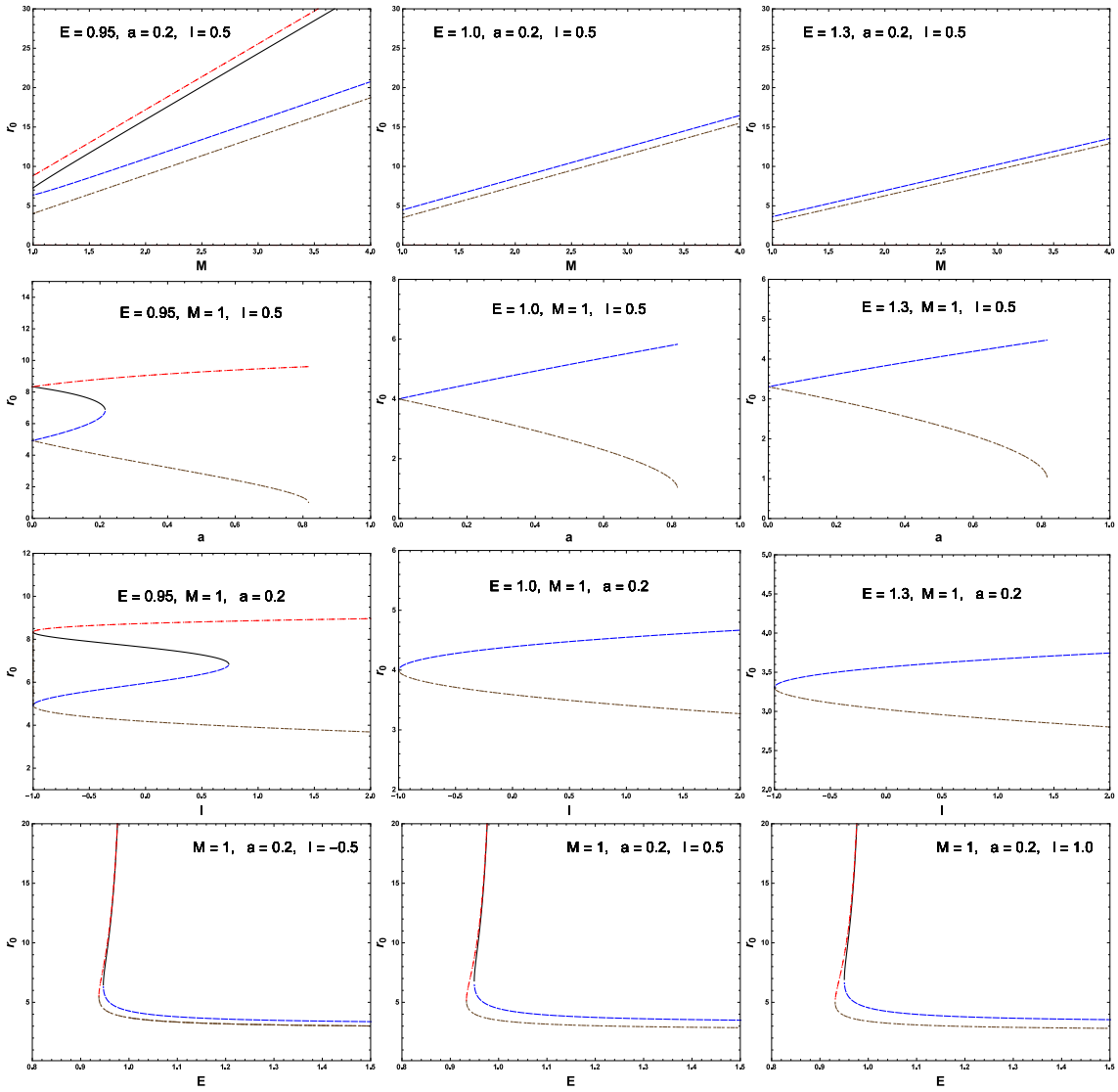


FIG. 2: The change of the circular orbit radius r_0 with the black hole parameters M, a, l and the particle's energy E in the rotating black hole spacetime (4) in Einstein-bumblebee theory. In each panel, the red or black line denotes the unstable orbit, the blue or brown line corresponds to the stable orbit.

stable co-rotating orbit and the stable counter-rotating one, respectively. With the increase of black hole mass parameter M, the radius r_0 for each circular orbit is an increasing function of black hole mass parameter M as $a = 0.2$ and $l = 0.5$. With the increasing spin parameter a, the radius r_0 for the unstable co-rotating orbit and the stable counter-rotating orbit increases, but deceases for the another two orbits. As in the previous discussion, Fig.(2) also shows that the change of r_0 with the parameter l is similar to that with a. From Fig.(2), as $E \geq 1$, we find that the radius r_0 for both of circular orbits decreases with E. However, as $E < 1$, the radius r_0 for two stable circular orbits decrease with E, but increases for another two unstable orbits.

Let us now focus on the stable circular orbits and assume some small perturbations around a stable circular orbit $r = r_0$ in the equatorial plane [38–51], i.e.,

$$r(t) = r_0 + \delta r(t), \qquad \theta(t) = \frac{\pi}{2} + \delta\theta(t). \tag{30}$$

Inserting the above perturbations into Eq.(11), one can find that the perturbations $\delta r(t)$ and $\delta\theta(t)$ satisfy the following differential equations

$$\frac{d^2\delta r(t)}{dt^2} + \Omega_r^2 \delta r(t) = 0, \qquad \frac{d^2\delta\theta(t)}{dt^2} + \Omega_\theta^2\, \delta\theta(t) = 0, \tag{31}$$

with

$$\Omega_r^2 = -\frac{1}{2g_{rr}\dot{t}^2}\frac{\partial^2 V_{eff}}{\partial r^2}\bigg|_{r=r_0,\theta=\frac{\pi}{2}}, \qquad \Omega_\theta^2 = -\frac{1}{2g_{\theta\theta}\dot{t}^2}\frac{\partial^2 V_{eff}}{\partial \theta^2}\bigg|_{r=r_0,\theta=\frac{\pi}{2}}. \tag{32}$$

The radial epicyclic frequency ν_r and the vertical epicyclic frequency ν_θ can be written as $\nu_r = \Omega_r/2\pi$ and $\nu_\theta = \Omega_\theta/2\pi$, respectively. Inserting metric functions (4) into Eq.(17) , we can find the azimuthal frequency

$$\nu_\phi = \frac{1}{2\pi}\frac{M^{1/2}}{r_0^{3/2} + a^* M^{3/2}\sqrt{l+1}}, \tag{33}$$

where $a^* \equiv a/M$. It is easy to find that the azimuthal frequency ν_ϕ decreases with the Lorentz symmetry breaking parameter l for the rotating case. From Eq.(17), one can find that this behavior of ν_ϕ with l is dominated by the derivatives $g_{\phi\phi,r}$ and $g_{t\phi,r}$ which increase with l in the equatorial plane. As $a = 0$, one can find that ν_ϕ is independent of the parameter l. Similarly, substituting metric functions (4) into Eqs.(19) and (32), one has

$$\nu_r = \nu_\phi\left[\frac{1}{l+1} - \frac{6M}{(l+1)r_0} + \frac{8a^* M^{3/2}}{\sqrt{l+1}r_0^{3/2}} - 3a^{*2}\frac{M^2}{r_0^2}\right]^{1/2}, \tag{34}$$

$$\nu_\theta = \nu_\phi\left[1 - \frac{4a^*\sqrt{l+1}M^{3/2}}{r_0^{3/2}} + 3a^{*2}(l+1)\frac{M^2}{r_0^2}\right]^{1/2}. \tag{35}$$

Obviously, in the rotating case $a \neq 0$, the frequencies ν_r and ν_θ depend on the Lorentz symmetry breaking parameter l. However, in the non-rotating case, one can find that only the frequency ν_r is related to the

parameter l since ν_θ is identical with ν_ϕ in this case with $a = 0$ and they are not functions of the parameter l. The properties of above three frequencies make it possible to constrain effect from the Lorentz symmetry breaking by quasi-periodic oscillations. As $l = 0$, it is easy to find that these three frequencies reduce to those in the usual Kerr black hole spacetime [32–35]. It is well known that the effective potential (12) plays an important role in determining the circular orbit's radius of particle and the corresponding frequencies of motions. From Eq.(32), the frequencies ν_r and ν_θ are determined by the second derivatives of the effective potential (12) together with a factor related to metric function and $\dot{t}^2$. In Fig.(3), we show the change of the partial derivatives $\frac{\partial^2 V_{eff}}{\partial r^2}|_{\theta=\frac{\pi}{2}}$, $\frac{\partial^2 V_{eff}}{\partial \theta^2}|_{\theta=\frac{\pi}{2}}$, and the factors $\frac{1}{g_{rr}\dot{t}^2}|_{\theta=\frac{\pi}{2}}$, $\frac{1}{g_{\theta\theta}\dot{t}^2}|_{\theta=\frac{\pi}{2}}$ with l for fixed $r_0 = 6.5$. It is shown that the absolute value of $\frac{\partial^2 V_{eff}}{\partial r^2}|_{\theta=\frac{\pi}{2}}$ increases with l, but the factor $\frac{1}{g_{rr}\dot{t}^2}|_{\theta=\frac{\pi}{2}}$ decreases. However, the effect of the second derivative $\frac{\partial^2 V_{eff}}{\partial r^2}|_{\theta=\frac{\pi}{2}}$ is suppressed by the factor $\frac{1}{g_{rr}\dot{t}^2}|_{\theta=\frac{\pi}{2}}$, which leads to that the frequency ν_r decreases with the parameter l. Since both the absolute value of $\frac{\partial^2 V_{eff}}{\partial r^2}|_{\theta=\frac{\pi}{2}}$ and $\frac{1}{g_{rr}\dot{t}^2}|_{\theta=\frac{\pi}{2}}$ increase with a, it is easy to obtain that the frequencies ν_r increases with a. Moreover, from Fig.(3), we also find that the second derivative $\frac{\partial^2 V_{eff}}{\partial \theta^2}|_{\theta=\frac{\pi}{2}}$ dominates the change of frequency ν_θ and results in that ν_θ is a decreasing function of l and a. Furthermore, the periastron and nodal precession frequencies can be expressed as

$$\nu_{\rm per} = \nu_\phi - \nu_r, \qquad \nu_{\rm nod} = \nu_\phi - \nu_\theta, \tag{36}$$

respectively. In Fig.(4), we plot the change of the frequencies ν_ϕ, ν_{per} and ν_{nod} for the rotating black hole spacetime in Einstein-bumblebee theory (4). It is shown that in the case with $a \neq 0$ the azimuthal frequency ν_ϕ decreases with l as in the previous discussion. Comparing Fig.(3) with Fig.(4), one can find that the frequencies ν_r and ν_θ decrease more rapidly than ν_ϕ, which yields that both of the periastron and nodal precession frequencies (ν_{per} and ν_{nod}) increase with the Lorentz symmetry breaking parameter l. Thus, the changes of ν_{per} and ν_{nod} with l are determined by the effective potential combined with the factor related to metric function and $\dot{t}^2$. We also find that as $a = 0$ the nodal precession frequency ν_{nod} is zero for arbitrary l as expected. With the increase of the spin parameter a, the frequencies ν_ϕ and ν_{per} decrease, but the frequency ν_{nod} increases.

According to the relativistic precession model, three simultaneous quasi-periodic oscillations frequencies are generated at the same radius of the orbit in the accretion flow. For a rotating black hole spacetime (4) in Einstein-bumblebee gravity, there are three parameters to describe black hole spactime. Thus, we have to resort to the χ^2 analysis and fit the values of these variables. Here, we adopt the observed data from black

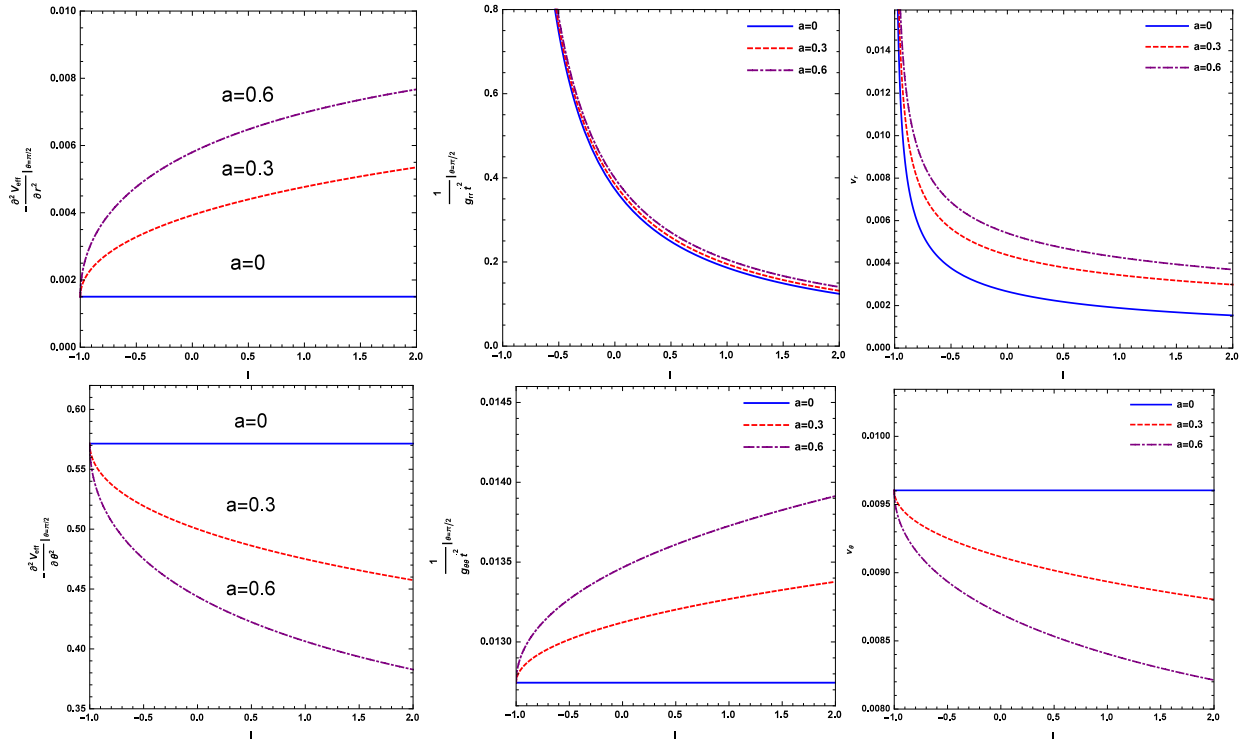


FIG. 3: The change of the second partial derivatives $-\frac{\partial^2 V_{eff}}{\partial r^2}|_{\theta=\frac{\pi}{2}}$, $-\frac{\partial^2 V_{eff}}{\partial \theta^2}|_{\theta=\frac{\pi}{2}}$, and the coefficients $\frac{1}{g_{rr}\dot{t}^2}|_{\theta=\frac{\pi}{2}}$, $\frac{1}{g_{\theta\theta}\dot{t}^2}|_{\theta=\frac{\pi}{2}}$ and the frequencies ν_r, ν_θ with the parameter l in the rotating black hole spacetime in Einstein-bumblebee theory. Here we set $M = 1$ and $r = 6.5$.

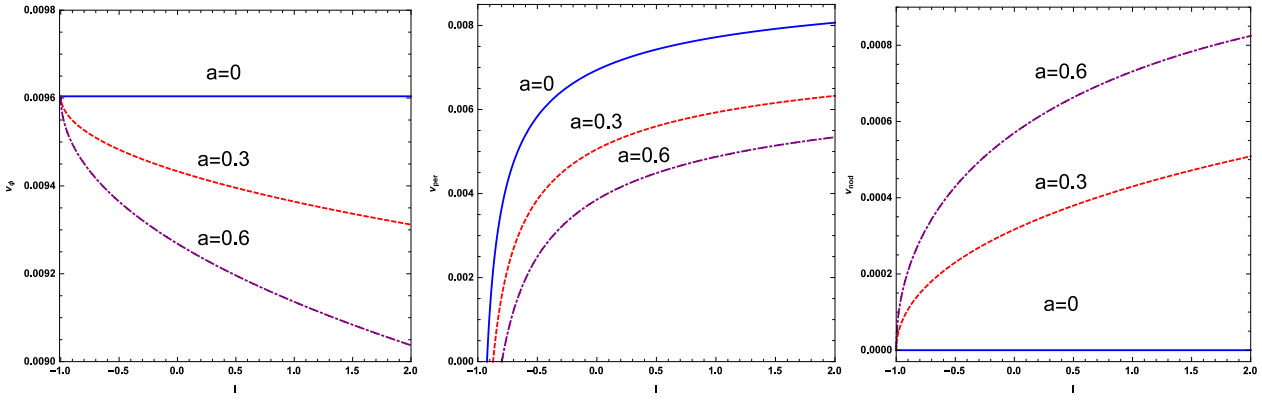


FIG. 4: The change of the frequencies ν_ϕ, ν_{per} and ν_{nod} with the parameter l in the rotating black hole spacetime in Einstein-bumblebee theory. Here we set $M = 1$ and $r = 6.5$.

hole sources exhibiting high frequency quasi-periodic oscillations, which are listed in Table I. From the current observations of GRO J1655-40, there are two set of data about these frequencies ($\nu_\phi, \nu_{\rm per}, \nu_{\rm nod}$)[32, 38]. Two set of frequencies can be regarded to be emitted by the relativistic particles moving along the orbits with the different radius r_1 and r_2, respectively. Moreover, the mass of the black hole is also independently measured by a dynamical method [42]: $M_{\rm dyn} = 5.4 \pm 0.3 M_\odot$. For the black hole sources XTE J1550-564 and GRS 1915+105, there are only the high frequencies data and the low frequency parts are lacking. With the data

	ν_ϕ	$\nu_{\rm per}$	$\nu_{\rm nod}$	$M/M_\odot$
GRO J1655-40	441 ± 2[32]	298 ± 4 [32]	17.3 ± 0.1[32]	5.4 ± 0.3 [42]
	451 ± 5 [32]	—	18.3 ± 0.1 [32]	
XTE J1550-564	276 ± 3[51]	184 ± 5 [51]	—	9.1 ± 0.61 [52]
GRS 1915+105	168 ± 3 [51]	113 ± 5 [51]	—	$12.4^{+2.0}_{-1.8}$ [53]

TABLE I: Data of quasi-periodic oscillations and black hole mass for GRO J1655-40, XTE J1550-564, and GRS 1915+105, respectively.

	$M/M_\odot$	a^*	l	r/M
GRO J1655-40	$5.4002^{+0.0478}_{-0.0562}$	$0.2976^{+0.0233}_{-0.0119}$	$-0.1048^{+0.1678}_{-0.1316}$	$r_1 = 5.6194^{+0.0346}_{-0.0334}$ $r_2 = 5.5154^{+0.0476}_{-0.0474}$
XTE J1550-564	$9.100^{+0.2450}_{-1.1443}$	$0.3697^{+0.4536}_{-0.0436}$	$-0.2053^{+6.7573}_{-0.3635}$	$5.4030^{+0.1010}_{-0.4050}$
GRS 1915+105	$12.4000^{+0.7400}_{-3.3580}$	$0.3080^{+3.7760}_{-0.3192}$	$1.3083^{+9.5717}_{-2.0134}$	$6.101^{+0.2566}_{-1.4794}$

TABLE II: Best-fit values and their range of 1σ for the black hole parameters with the metric (4) from GRO J1655-40, XTE J1550-564, and GRS 1915+105, respectively.

listed in Table I, we can constrain the parameters of a rotating black hole spacetime (4) in Einstein-bumblebee gravity through the relativistic precession model as in ref.[38]. Together with the χ^2 analysis, we can fit the parameters of black hole (4) in Einstein-bumblebee gravity. The best-fit values and their range of 1σ for the black hole parameters are listed in Table II. The Table II shows that the circular orbit of quasi-periodic oscillations lies in the strong gravitational-field region of the black hole. In Fig.5, we show the contour levels of 1σ, 2σ and 3σ for the black hole parameters M, a and l with different observed black hole sources. Comparing with the constraint results obtained by data of three black hole sources, presented in Table II and Fig.5, we find that the 1σ region of l obtained by GRO J1655-40 data is the most narrow and it also lies in the 1σ regions obtained by the other two black hole sources, which means that the constraint on the Lorentz symmetry breaking parameter l is more precise with data of GRO J1655-40. The main reason may be that there are more available observation data of quasi-periodic oscillations for GRO J1655-40.

According to the constraint from GRO J1655-40, the best-fit value of $l = -0.1048$ is negative, which means that the spacetime described gravitational field in the Einstein-bumblebee gravity (4) should allow $|a|/M > 1$

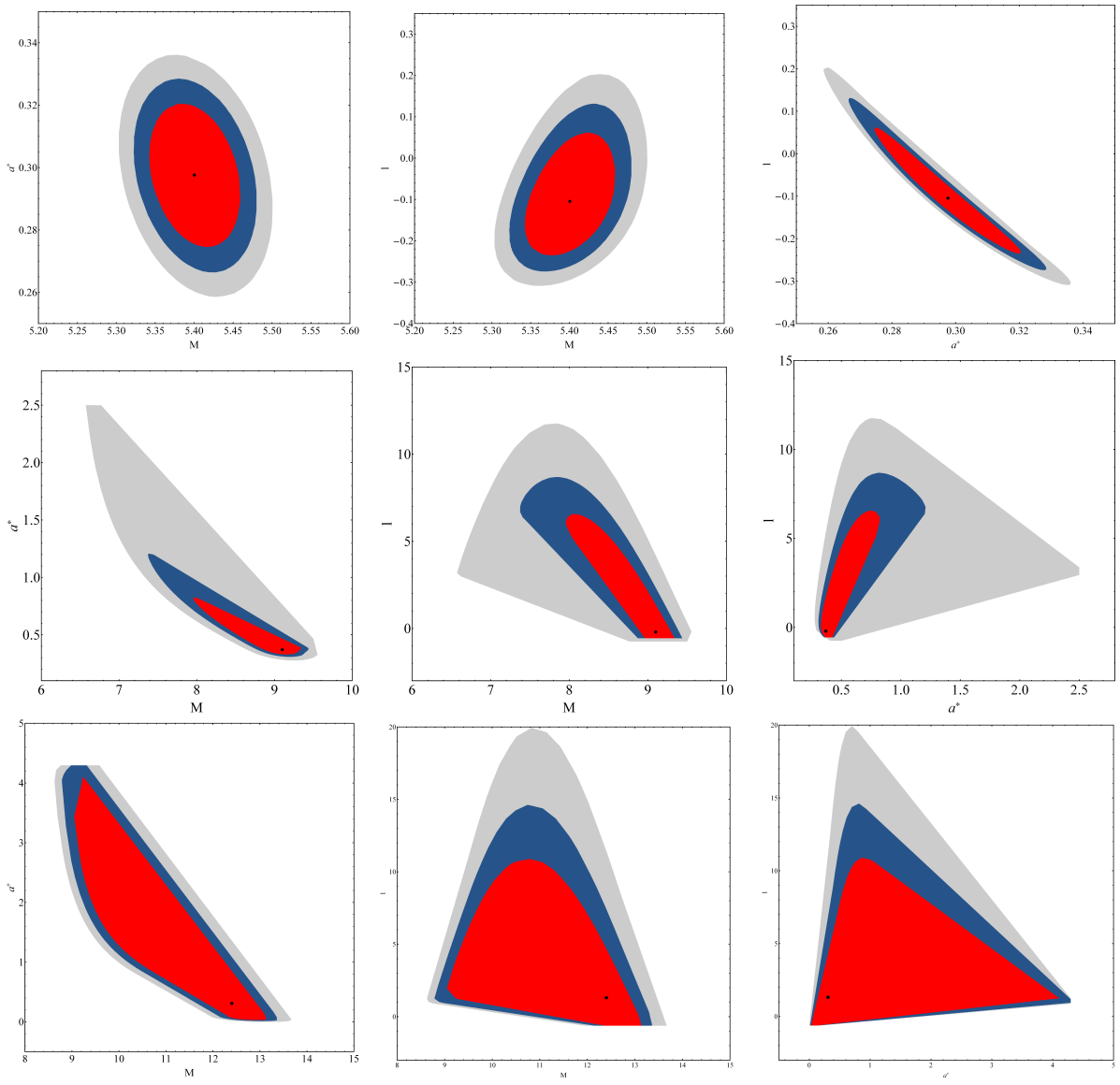


FIG. 5: Constraints on the parameters of the rotating black hole in Einstein-bumblebee theory (4) from current observations of QPOs within the relativistic precession model. The top, middle and bottom rows correspond to the constraint from GRO J1655-40, XTE J1550-564, and GRS 1915+105, respectively. The red, blue and gray regions in the panels represent the contour levels 1σ, 2σ and 3σ, respectively. The black dots denote the best-fit values of black hole parameters.

for a black hole. It implies that the range of black hole spin parameter a is larger than that in the Kerr case in general relativity. Comparing with the usual Kerr black hole spacetime, the negative l leads to that both the outer ergosurface radius r_{outerg} and the outer horizon radius r_+ increase, but the width between the outer ergosurface and the outer horizon $r_{outerg} - r_+ = \frac{a^2 \sin^2\theta}{\sqrt{M^2-(l+1)a^2}+\sqrt{M^2-(l+1)a^2\cos^2\theta}}$ decreases for fixed θ, which yields the lower possibility of exacting energy by Penrose process for a rotating black hole in Einstein-bumblebee gravity (4). Moreover, the negative l means that the black hole (4) owns the higher Hawking temperature and the stronger Hawking radiation than the Kerr black hole. From Table II and Fig.(2), we find

that the case of $l = 0$ lies in the range of 1σ obtained by three black hole sources, which means that general relativity remains to be consistent with the observation data of quasi-periodic oscillations frequencies.

IV. SUMMARY

With relativistic precession model, we have studied quasi-periodic oscillations frequencies in a rotating black hole in Einstein-bumblebee gravity (4). The black hole owns three parameters: mass M, spin a and the Lorentz symmetry breaking parameter l. We find that in the case with $a \neq 0$ both of the periastron and nodal precession frequencies (ν_{per} and ν_{nod}) increase with the Lorentz symmetry breaking parameter l, but the azimuthal frequency ν_ϕ decreases. In the non-rotating black hole case, the nodal precession frequency ν_{nod} is zero for arbitrary l since $\nu_\theta = \nu_\phi$ in this case and they are independent of the parameter l. With the increase of the spin parameter, the frequencies ν_ϕ and ν_{per} decrease, but the frequency ν_{nod} increases. With the observation data of GRO J1655-40, XTE J1550-564, and GRS 1915+105, we constrain the parameters of the rotating black hole in Einstein-bumblebee gravity (4), respectively. Our results show that the constraint on the Lorentz symmetry breaking parameter l is more precise with data of GRO J1655-40. According to the constraint from GRO J1655-40, one can find that the best-fit value of the Lorentz symmetry breaking parameter l is negative. Comparing with the usual Kerr spacetime, the negative l leads to that the black hole (4) in Einstein-bumblebee gravity owns the higher Hawking temperature and the stronger Hawking radiation than the Kerr black hole, but the lower possibility of exacting energy by Penrose process. However, in the range of 1σ, general relativity (where$l = 0$) remains to be consistent with the observation data of GRO J1655-40, XTE J1550-564 and GRS 1915+105.

V. ACKNOWLEDGMENTS

This work was supported by the National Natural Science Foundation of China under Grant No.11875026, 11875025, 12035005 and 2020YFC2201403.

VI. APPENDIX

In this section, we present the derivation of the equation (23) for the circular orbit r_0. The effective potential (13) can be written as

$$V_{eff} \equiv \frac{A(r)}{B(r)} - 1, \tag{37}$$

with

$$A(r) \equiv [r^3 + (r+2M)(l+1)a^2]E^2 - 4aM\sqrt{l+1}EL_z - (r-2M)L_z^2,$$
$$B(r) \equiv r[r^2 - 2Mr + (l+1)a^2]. \tag{38}$$

From the conditions (21) of the circular orbit, one can obtain

$$A(r_0) = B(r_0), \qquad A(r_0)B'(r_0) - A'(r_0)B(r_0) = 0. \tag{39}$$

It means that $A'(r_0) = B'(r_0)$, which gives directly the equation (22). Substituting it into the above equations (39), one can get the equation (23) satisfied by the circular orbit r_0 in the equatorial plane.

[1] G. T. Zatsepin and V. A. Kuzmin, *Upper limit of the spectrum of cosmic rays*, JETP Lett. **4**, 78 (1966).

[2] M. Takeda et al., *Extension of the cosmic ray energy spectrum beyond the predicted Greisen-Zatsepin-Kuz'min cutoff*, Phys. Rev. Lett. **81**, 1163 (1998); [astro-ph/9807193].

[3] R. Casana, A. Cavalcante, F.P. Poulis and E.B. Santos, *Exact Schwarzschild-like solution in a bumblebee gravity model*, Phys. Rev. D **97**, 104001 (2018) [arXiv:1711.02273].

[4] V. Kostelecky and S. Samuel, *Gravitational Phenomenology in Higher Dimensional Theories and Strings*, Phys. Rev. D **40**, 1886(1989).

[5] V. Kostelecky and S. Samuel, *Spontaneous breaking of Lorentz symmetry in string theory*, Phys. Rev. D **39**, 683 (1989).

[6] R. Bluhm and V.A. Kostelecky, *Spontaneous Lorentz violation, Nambu-Goldstone modes, and gravity*, Phys. Rev. D **71**, 065008 (2005), [hep-th/0412320.

[7] O. Bertolami and J. Paramos, *The Flight of the bumblebee: Vacuum solutions of a gravity model with vector-induced spontaneous Lorentz symmetry breaking*, Phys. Rev. D **72**, 044001 (2005) [hep-th/0504215].

[8] Q. G. Bailey and V. Kostelecky, *Signals for Lorentz violation in post-Newtonian gravity*, Phys. Rev. D **74**, 045001 (2006),[gr-qc/0603030].

[9] R. Bluhm, N. L. Gagne, R. Potting and A. Vrublevskis, *Constraints and Stability in Vector Theories with Spontaneous Lorentz Violation*, Phys. Rev. D **77**, 125007 (2008); [Erratum ibid. **79** 029902 (2009) [arXiv:0802.4071].

[10] V. Kostelecky and J. Tasson, *Prospects for Large Relativity Violations in Matter-Gravity Couplings*, Phys. Rev. Lett. **102**, 010402 (2009) [arXiv:0810.1459].

[11] M. D. Seifert, *Generalized bumblebee models and Lorentz-violating electrodynamics*, Phys. Rev. D **81**, 065010 (2010), [arXiv:0909.3118].

[12] R.V. Maluf, C.A.S. Almeida, R. Casana and M. Ferreira, *Einstein-Hilbert graviton modes modified by the Lorentz-violating bumblebee Field*, Phys. Rev. D **90**, 025007 (2014) [arXiv:1402.3554].

[13] J. Páramos and G. Guiomar, *Astrophysical Constraints on the Bumblebee Model*, Phys. Rev. D **90**, 082002 (2014), [arXiv:1409.2022],.

[14] C.A. Escobar and A. Martín-Ruiz, *Equivalence between bumblebee models and electrodynamics in a nonlinear gauge*, Phys. Rev. D **95**, 095006 (2017), [arXiv:1703.01171].

[15] J.F. Assunão, T. Mariz, J.R. Nascimento and A.Y. Petrov, *Dynamical Lorentz symmetry breaking in a tensor bumblebee model*, Phys. Rev. D **100**, 085009 (2019), [arXiv:1902.10592].

[16] A. Ovgun, K. Jusufi and I. Sakalli, *Gravitational Lensing Under the Effect of Weyl and Bumblebee Gravities: Applications of Gauss-Bonnet Theorem*, Annals Phys. **399**, 193 (2018) [arXiv:1805.09431].

[17] S. Kanzi and I. Sakalli, *GUP Modified Hawking Radiation in Bumblebee Gravity*, Nucl. Phys. B **946**, 114703 (2019) [arXiv:1905.00477].

[18] R. Oliveira, D. M. Dantas, and C. A. S. Almeida, *Quasinormal frequencies for a black hole in a bumblebee gravity*, EPL **135** 1, 10003 (2021), arXiv:2105.07956 [gr-qc].

[19] I. Güllü and A. Övgün, (2020), *Schwarzschild Like Solution with Global Monopole in Bumblebee Gravity*, arXiv:2012.02611 [gr-qc].

[20] R. V. Maluf and J. C. S. Neves, *Black holes with a cosmological constant in bumblebee gravity*, Phys. Rev. D 103, 044002 (2021).

[21] C. Ding, X. Chen, and X. Fu, *Einstein-Gauss-Bonnet gravity coupled to bumblebee field in four dimensional spacetime*, arXiv:2102.13335 [gr-qc].

[22] A. Övgün, K. Jusufi and I. Sakall, *Exact traversable wormhole solution in bumblebee gravity*, Phys. Rev. D **99**, 024042 (2019), [arXiv:1804.09911].

[23] D. Capelo and J. Páramos, *Cosmological implications of Bumblebee vector models*, Phys. Rev. D **91**, 104007 (2015) [arXiv:1501.07685].

[24] C. Ding, C. Liu, R. Casana and A. Cavalcante, *Exact Kerr-like solution and its shadow in a gravity model with spontaneous Lorentz symmetry breaking*, Eur. Phys. J. C **80**, 178 (2020), [arXiv:1910.02674]

[25] H. Wang, S. Wei, textitShadow cast by Kerr-like black hole in the presence of plasma in Einstein-bumblebee gravity, arXiv:2106.14602

[26] C. Liu, C. Ding and J. Jing, *Thin accretion disk around a rotating Kerr-like black hole in Einstein-bumblebee gravity model*, arXiv:1910.13259 .

[27] R. Jiang, R. Lin, X. Zhai, *Superradiant instability of the Kerr-like black hole in Einstein-bumblebee gravity*, Phys. Rev. D **104**, 124004 (2021), arXiv: 2108.04702 [gr-qc]

[28] Z. Li and A. Övgün, *Finite-distance gravitational deflection of massive particles by a Kerr-like black hole in the bumblebee gravity model*, Phys. Rev. D **101**, 024040 (2020).[arXiv:2001.02074].

[29] S. K. Jha and A. Rahaman, *Bumblebee gravity with a Kerr-Sen-like solution and its Shadow*, Eur. Phys. J. C **81**, 345 (2021), arXiv:2011.14916 [gr-qc].

[30] R. A. Remillard and J. E. McClintock, *X-ray Properties of Black-Hole Binaries*, Ann. Rev. Astron. Astrophys. **44**, 49 (2006).

[31] T. M. Belloni and S. E. Motta, *Transient Black Hole Binaries*, arXiv:1603.07872.

[32] S. E. Motta, T. M. Belloni, L. Stella, T. Muoz-Darias and R. Fender, *Precise mass and spin measurements for a stellar-mass black hole through X-ray timing: the case of GRO J1655-40*, Mon. Not. Roy. Astron. Soc. **437**, 2554 (2014) [arXiv:1309.3652 [astro-ph.HE]].

[33] S. E. Motta, T. Muoz-Darias, A. Sanna, R. Fender, T. Belloni and L. Stella, *Black hole spin measurements through the relativistic precession model: XTE J1550-564*, Mon. Not. Roy. Astron. Soc. **439**, 65 (2014) [arXiv:1312.3114

[astro-ph.HE]].

[34] P. Casella, T. Belloni, and L. Stella, *The ABC of low-frequency quasi-periodic oscillations in black-hole candidates: Analogies with Z-sources*, Astrophys. J. **629**, 403 (2005).

[35] L. Stella and M. Vietri, *Lense-Thirring Precession and QPOs in Low Mass X-Ray Binaries* , Astrophys. J. **492**, L59 (1998) [astro-ph/9709085]

[36] L. Stella and M. Vietri, *kHz Quasi Periodic Oscillations in Low Mass X-ray Binaries as Probes of General Relativity in the Strong Field Regime* , Phys. Rev. Lett. **82**, 17 (1999) [astro-ph/9812124].

[37] L. Stella, M. Vietri and S. Morsink, *Correlations in the QPO Frequencies of Low Mass X-Ray Binaries and the Relativistic Precession Model* , Astrophys. J. **524**, L63 (1999) [astro-ph/9907346].

[38] C. Bambi, *Probing the space-time geometry around black hole candidates with the resonance models for high-frequency QPOs and comparison with the continuum-fitting method*, J. Cosmol. Astropart. Phys. **1209**, 014 (2012)

[39] C. Bambi and S. Nampalliwar, *Quasi-periodic oscillations as a tool for testing the Kerr metric: A comparison with gravitational waves and iron line*,Europhys. Lett. **116**, 30006 (2016), arXiv:1604.02643.

[40] Z. Stuchlik and A. Kotrlova, *Orbital resonances in discs around braneworld Kerr black holes*, Gen. Rel. Grav. **41**, 1305 (2009).

[41] T. Johannsen and D. Psaltis, *Testing the No-Hair Theorem with Observations in the Electromagnetic Spectrum. III. Quasi-Periodic Variability*, Astrophys. J. **726**, 11 (2011) [arXiv:1010.1000 [astro-ph.HE]].

[42] M. E. Beer and P. Podsiadlowski, *The quiescent light curve and evolutionary state of GRO J1655-40*, Mon. Not. Roy. Astron. Soc. **331**, 351 (2002) [astro-ph/0109136].

[43] A. Maselli, L. Gualtieri, P. Pani, L. Stella, and V. Ferrari, *Testing Gravity with Quasi Periodic Oscillations from accreting Black Holes: the Case of Einstein-Dilaton-Gauss-Bonnet Theory*, Astrophys. J. **801**, 115 (2015).

[44] A. G. Suvorov and A. Melatos, *Testing modified gravity and no-hair relations for the Kerr-Newman metric through quasiperiodic oscillations of galactic microquasars*, Phys. Rev. D **93**, 024004 (2016).

[45] G. Pappas, *What can quasi-periodic oscillations tell us about the structure of the corresponding compact objects?*, Mon. Not. R. Astron. Soc. **422**, 2581-2589 (2012).

[46] K. Boshkayev, D. Bini, J. Rueda, A. Geralico, M. Muccino and I. Siutsou, *What can we extract from quasiperiodic oscillations?*, Grav. Cosmol. **20**, 233-239 (2014).

[47] S. Chen, M. Wang, J.Jing, *Testing gravity of a regular and slowly rotating phantom black hole by quasiperiodic oscillations*, Class. Quantum Grav. **33**, 195002 (2016).

[48] A. Allahyari, L. Shao, *Testing No-Hair Theorem by Quasi-Periodic Oscillations: the quadrupole of GRO J1655-40*, J. Cosmol. Astropart. Phys. **10**, 003 (2021), arXiv: 2102.02232.

[49] A. Maselli, L. Gualtieri, P. Pani, L. Stella, V. Ferrari, *Testing Gravity with Quasi Periodic Oscillations from accreting Black Holes: the Case of Einstein-Dilaton-Gauss-Bonnet Theory*, Astrophys. J. **801** 2, 115 (2015).

[50] S. Chen, Z. Wang and J. Jing, *Testing gravity of a disformal Kerr black hole in quadratic degenerate higher-order scalar-tensor theories by quasi-periodic oscillations* , J. Cosmol. Astropart. Phys. **06**, 043 (2021), arXiv: 2103.11788.

[51] I. Banerjee, S. Chakraborty, S. SenGuptab, *Looking for extra dimensions in the observed quasi-periodic oscillations of black holes*, J. Cosmol. Astropart. Phys. **09**, 037 (2021), arXiv: 2105.06636.

[52] J. A. Orosz *et al.*, *An Improved Dynamical Model for the Microquasar XTE J1550-564*, Astrophys. J. **730**, 75 (2011) [arXiv:1101.2499].

[53] M. J. Reid *et al.*, *A Parallax Distance to the Microquasar GRS 1915+105 and a Revised Estimate of its Black Hole Mass*, Astrophys. J. **796**, 2 (2014) [arXiv:1409.2453].